

The double-funnel energy landscape of the 38-atom Lennard-Jones cluster

Jonathan P. K. Doye

University Chemical Laboratory, Lensfield Road, Cambridge CB2 1EW, United Kingdom and FOM Institute for Atomic and Molecular Physics, Kruislaan 407, 1098 SJ Amsterdam, The Netherlands

Mark A. Miller and David J. Wales

University Chemical Laboratory, Lensfield Road, Cambridge CB2 1EW, United Kingdom

(Received 2 September 1998; accepted 29 December 1998)

The 38-atom Lennard-Jones cluster has a paradigmatic double-funnel energy landscape. One funnel ends in the global minimum, a face-centered-cubic (fcc) truncated octahedron. At the bottom of the other funnel is the second lowest energy minimum which is an incomplete Mackay icosahedron. We characterize the energy landscape in two ways. First, from a large sample of minima and transition states we construct a disconnectivity graph showing which minima are connected below certain energy thresholds. Second, we compute the free energy as a function of a bond-order parameter. The free energy profile has two minima, one which corresponds to the fcc funnel and the other which at low temperature corresponds to the icosahedral funnel and at higher temperatures to the liquidlike state. These two approaches show that the greater width of the icosahedral funnel, and the greater structural similarity between the icosahedral structures and those associated with the liquidlike state, are the cause of the smaller free energy barrier for entering the icosahedral funnel from the liquidlike state and therefore of the cluster's preferential entry into this funnel on relaxation down the energy landscape. Furthermore, the large free energy barrier between the fcc and icosahedral funnels, which is energetic in origin, causes the cluster to be trapped in one of the funnels at low temperature. These results explain in detail the link between the double-funnel energy landscape and the difficulty of global optimization for this cluster. © 1999 American Institute of Physics. [S0021-9606(99)50113-X]

I. INTRODUCTION

Understanding the relationship between the potential energy surface (PES), or energy landscape, and the dynamics of a complex system is a major research effort in the chemical physics community. For example, much theoretical work has attempted to find the features of the energy landscape which differentiate those model polypeptides that are able to fold rapidly to a unique native structure from those that get stuck in misfolded states.¹⁻⁵ Similarly, the answers to a whole host of questions about glasses must lie in the energy landscape. Why are glasses unable to reach the crystalline state? What is the cause of the differences between "strong" and "fragile" liquids? What processes, at a microscopic level, are responsible for α and β relaxation?

A key concept that has arisen within the protein folding community is that of a funnel consisting of a set of downhill pathways that converge on a single low-energy minimum.^{6,7} It has been suggested that the PES's of proteins are characterized by a single deep funnel and that this feature underlies their ability to fold to their native state. Indeed it is easy to design model single-funnel PES's that result in efficient relaxation to the global minimum, despite very large configurational spaces.⁸⁻¹⁰ By contrast, polypeptides that misfold are expected to have other funnels that can act as traps. Attempts have been made to characterize the energy landscape of proteins in these terms through, for example, mapping the connections between compact states,^{6,11} disconnectivity graphs,¹²⁻¹⁴ monotonic sequences,¹⁵ and free energy

profiles.^{16,17} However, for the most part these studies have been limited either to simplified lattice models, where the most natural elementary division of the PES into basins of attraction surrounding local minima¹⁸ is problematic, or to short polypeptides if more realistic models are used.

An intuitive picture of the energy landscape of glasses has also been proposed in which the crystal corresponds to a very narrow funnel which is inaccessible from the liquid.^{19,20} Most of the PES is dominated by rugged regions where there are many funnels leading to different amorphous structures. Therefore, the structure that the system relaxes to depends upon its thermal history. In this picture the different relaxation processes result from the hierarchy of barriers in the amorphous regions of the PES.²⁰ Although this picture is appealing, only recently has progress been made in relating the details of glassy behavior to the features of the PES.²¹⁻²³ This task is hampered by the complexity of the PES's for these systems; the number of minima is huge and characterization of the PES is hampered by the slow relaxation times.

In view of the complex energy landscapes of model proteins and glasses, it is also useful to have systems for which it is easier to understand the relationship between the PES and the dynamics. Clusters can provide such an alternative perspective. For example, the complexity of the PES (in terms of the number of minima) can be controlled through the cluster size^{24,25} and the choice of potential parameters, such as the range of attraction.^{26,27}

Clusters where the atoms interact through the Lennard-Jones (LJ) potential,

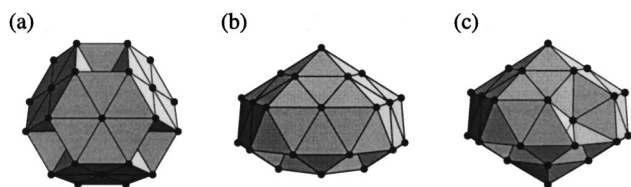


FIG. 1. (a) The LJ₃₈ global minimum, an fcc truncated octahedron ($E = -173.928\,427\epsilon$; point group O_h). (b) Second lowest energy minimum of LJ₃₈ ($E = -173.252\,378\epsilon$; point group C_{5v}). (c) Third lowest energy minimum ($E = -173.134\,317\epsilon$; point group C_s). The structures in (b) and (c) are both incomplete Mackay icosahedra.

$$E = 4\epsilon \sum_{i < j} \left[\left(\frac{\sigma}{r_{ij}} \right)^{12} - \left(\frac{\sigma}{r_{ij}} \right)^6 \right], \quad (1)$$

where ϵ is the pair well depth and $2^{1/6}\sigma$ is the equilibrium pair separation, provide a particularly useful model system, because their structure, thermodynamics and dynamics have been much studied. For small LJ clusters a complete enumeration of the minima and transition states allows a detailed view of the dynamics to be obtained.^{28,29}

At larger sizes, well-chosen examples allow one to consider particular paradigmatic types of energy landscape. For example, the PES of LJ₅₅ has a single deep funnel which leads down to the Mackay icosahedron³⁰ global minimum, and LJ₃₈, the cluster which we study here, has a double-funnel landscape. The LJ₃₈ global minimum is a face-centered-cubic (fcc) truncated octahedron^{31,32} [Fig. 1(a)] and the second lowest energy minimum is an incomplete Mackay icosahedron³³ [Fig. 1(b)]. These two minima lie at the bottom of separate funnels on the PES. The thermodynamics of this cluster have recently been characterized.^{34,35} At low temperature the truncated octahedron has the lowest free energy but, because the entropy associated with the icosahedral funnel is larger, its free energy becomes lower than that for the fcc funnel at about two-thirds of the melting temperature. Therefore, a transition takes place between the two states which is the finite-size equivalent of a solid-solid phase transition.

This thermodynamic transition affects the dynamics. Relaxation down the PES from the liquidlike state almost invariably leads into the icosahedral funnel. This is partly because, near to melting, icosahedral structures have a lower free energy than fcc structures. However, entry into the icosahedral funnel also seems to be dynamically favored, perhaps because of the greater structural similarity between the icosahedral and liquidlike structures—both have some polytetrahedral character.^{8,26,36} One aim of this paper is to characterize in detail the reasons for the greater accessibility of the icosahedral funnel.

Furthermore, once the cluster enters the icosahedral funnel it becomes trapped there, even when the free energy of the fcc funnel is lower. There is a large free energy barrier between the two funnels which prevents the cluster passing between them, but the nature and size of this barrier have not yet been probed.

These features make global optimization of this system much more difficult than for most small LJ clusters; most have global minima based on the Mackay icosahedra with no

other competitive morphologies.³⁷ Indeed, the LJ₃₈ global minimum was initially discovered on the basis of physical insight.³¹ Although the truncated octahedron has since been found by a number of global optimization methods,^{32,33,38–41} most of these techniques examine not the usual LJ energy landscape, but a landscape that has been transformed with the aim of making global optimization easier. The basis for the success of one of these methods lies in the significant changes to the thermodynamics and dynamics that the transformation causes.^{34,35}

We use two tools to characterize the double-funnel topography of the LJ₃₈ PES; in Sec. II we use a disconnectivity graph, and in Sec. III we examine the free energy landscape. Some of the results presented here have previously appeared in a short communication.⁴²

II. DISCONNECTIVITY GRAPH

To examine the topography of the PES, we need to locate its minima and the network of transition states and pathways that connect them. A transition state is a stationary point on the PES where the Hessian matrix has exactly one negative eigenvalue. Transition states can be found efficiently using eigenvector-following,^{43–45} in which the energy is maximized along one direction and simultaneously minimized along all others. The minima connected to a transition state are defined by the end-points of the steepest-descent paths commencing parallel and antiparallel to the transition vector (the eigenvector whose eigenvalue is negative). For this calculation we employ a method that uses analytic second derivatives.⁴⁶

The number of locally stable structures that LJ₃₈ can adopt is too large for it to be desirable or even possible to catalog them all. However, here we are primarily interested in the energetically low-lying regions of the PES associated with the two funnels. In recent years, a number of similar approaches for systematically exploring a PES by hopping between wells have been developed,^{25,47–49} and these are easily adapted to produce an algorithm that explores low-energy regions of the PES preferentially. In our scheme, we commence at a known low-lying minimum and proceed as follows:

- (1) Search for a transition state along the Hessian eigenvector with the smallest nonzero eigenvalue.
- (2) Find the steepest-descent pathway through the transition state and the two minima it connects, as described above.
- (3) There are various possible outcomes from step (2):
 - (a) In most cases, one of the connected minima is the minimum from which the transition state search was initiated. If this is the case, and the other minimum is lower in energy, we move to it.
 - (b) If the original minimum is one of the connected ones, but the other is higher in energy, the move is rejected.
 - (c) Sometimes the transition state is not connected to the minimum from which the search started. If neither minimum has been found previously, the pathway is then isolated from the rest of the database. Since we want to explore patterns of connec-

tivity in the low-energy regions of the PES, we discard the transition state and both minima under these circumstances. Such searches can be repeated later, when the database has grown and a connection may be found.

(d) If the original minimum is not connected, but one or both minima have already been visited, the pathway is recorded, but we remain at the original minimum.

- (4) The procedure continues from step (1), searching in both directions along eigenvectors with successively higher eigenvalues from the modified position.
- (5) When a specified number, n_{ev} , of eigenvectors of a minimum have been searched for transition states, the position jumps to the lowest-energy known minimum for which fewer than n_{ev} eigenvectors have been searched.

By only accepting downhill moves, this algorithm prevents the search becoming lost in the manifold of liquidlike minima. In the present work, we chose $n_{ev} = 10$, allowing up to 20 transition state searches from each minimum. In general, searches along eigenvectors with small eigenvalues are more likely to converge to transition states in a reasonable number of iterations. One can obtain an impression of how thoroughly the low-energy regions of the PES have been explored by monitoring how many of the lowest-energy minima are displaced as the search proceeds. Having collected 3000 minima, the next 1000 displaced only 6 of the previous lowest 200, and the next 2000 displaced only a further 7.

In the course of the search, several multiple-step paths between the low-lying O_h and C_{5v} minima emerged. The highest point on the lowest-energy path that we found was a transition state with energy -169.709ϵ (4.219ϵ above the global minimum); the path has an integrated length of 18.5σ . This demonstrates the efficiency of well-hopping techniques over more conventional methods for exploring a PES, such as molecular dynamics (MD); to restrict MD to regions of low potential energy, the total energy of the simulation would have to be low, and the trajectory would waste time undergoing intrawell oscillations, but at energies high enough to allow interfunnel passage at a reasonable rate, the trajectory could escape into the numerous liquidlike structures.

An informative way to visualize the PES and reveal funnel structure is to plot a disconnectivity graph.¹³ Such graphs have been used to obtain insight into the energy landscape of polypeptides,^{12–14} C_{60} ,^{42,50} and water,⁴² sodium chloride,⁵¹ and Morse²⁷ clusters. At a given total energy, E , minima can be grouped into disjoint sets, called basins, whose members are mutually accessible at that energy. In other words, each pair of minima in a basin are connected directly or through other minima by a path whose energy never exceeds E , but would require more energy to reach a minimum in another basin. At low energy there is just one basin, that containing the global minimum. At successively higher energies, more basins come into play as new minima are reached. At still higher energies, the basins coalesce as higher barriers are overcome, until finally there is just one basin containing all

the minima (provided there are no infinite barriers).

In a disconnectivity graph, the basin analysis is performed at a series of energies, which are plotted on a vertical axis. At each energy, a basin is represented by a node, and lines join nodes in one level to their daughter nodes in the level below. The horizontal position of a node has no significance, and is chosen for clarity. In these graphs an ideal funnel would appear as a single tall stem with branches sprouting directly from it at a series of levels, indicating the progressive exclusion of minima as the energy is decreased. Small clusters with a deep global minimum—such as LJ_{13} for which the global minimum is an icosahedron⁵²—closely approximate this ideal situation. For larger “single funnel” clusters, the graphs have the same basic shape but superimposed on this there is likely to be a certain amount of fine structure. For example, there might be sets of minima which have low barriers between them and so in the graph they are connected to each other before they connect to the stem of the global minimum. This is the case for LJ_{55} , for which the global minimum is a Mackay icosahedron.⁵² By contrast, a PES with a multiple-funnel topography would have two or more stems which split at high energy and lead down to different low energy minima. This splitting would mean that there is a large energy barrier to pass between the funnels and so the different funnels would be expected to possess distinct thermodynamic states.

Figure 2 shows the disconnectivity graph for LJ_{38} using a sample of 6000 minima and 8633 transition states, and a level spacing of 0.5ϵ . For clarity, only branches leading to the 150 lowest-energy minima are shown, but the number of minima that would be represented by some of the larger nodes are indicated. The graph confirms our assumption at the start of this paper that the LJ_{38} PES has two funnels. The large funnel associated with the icosahedral structures (placed centrally) is immediately visible. The lowest node connecting it to the funnel of the fcc global minimum lies at -169.5ϵ , so the 446 minima in the node below can be considered as belonging to the icosahedral funnel. In contrast, the funnel of the global minimum contains only 28 of the minima in our sample—over an order of magnitude fewer. Although only 150 branches are shown in the figure, one can see from the rapidly increasing density of branch-ends as the energy rises past -171.5ϵ , that the number of states available to the cluster increases dramatically with energy. This increase signifies the onset of the liquidlike part of the PES, and the disconnectivity graph shows that the system must enter this region of configuration space in order to pass between the icosahedral and fcc funnels.

The graph also gives an impression of the “shape” of the two funnels. The branches in the fcc funnel are generally longer than those in the icosahedral funnel, indicating higher barriers. Also, the global minimum is considerably lower in energy than the rest of the minima in the fcc funnel because it has a complete outer shell. In contrast to the fcc funnel, and to sizes at which a complete Mackay icosahedron can be formed,^{27,52} the bottom of the icosahedral funnel is not dominated by a single minimum. Rather there are many low-energy icosahedral minima associated with different ways of arranging the atoms in the incomplete surface layer. This

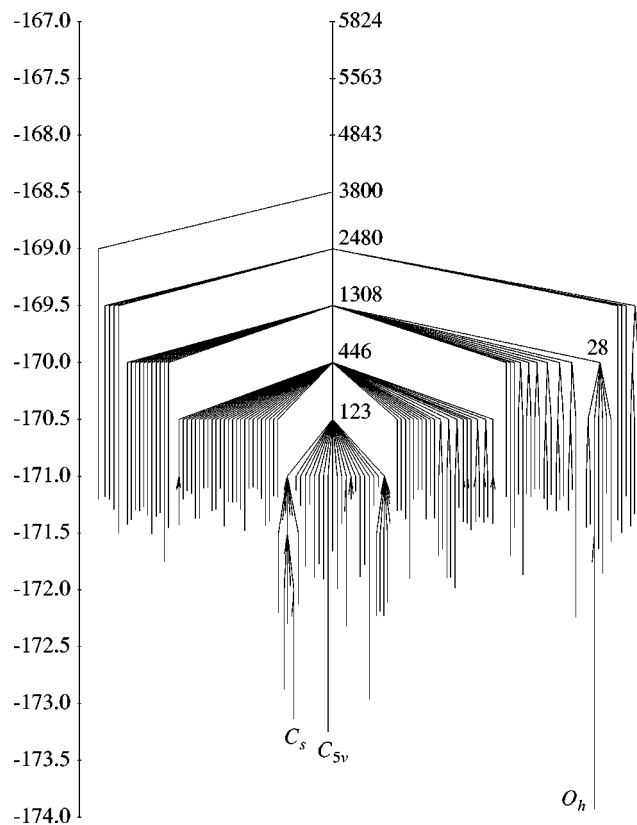


FIG. 2. Disconnectivity graph for LJ_{38} using a sample of 6000 minima and 8633 transition states. Only branches leading to the 150 lowest-energy minima are shown, but numbers attached to nodes indicate the number of minima they represent. The branches terminating at the three lowest-lying minima (see Fig. 1) are labeled by their point groups. The energy scale is in units of ϵ .

combined with the differing barrier heights between the minima gives rise to the structure at the bottom of the icosahedral funnel in the disconnectivity graph. For example, it is noticeable that the barriers about the low-lying C_s minimum [Fig. 1(c)] are lower than those for the C_{5v} minimum, indicating that rearrangement of the vacancy associated with the missing vertex atom is much easier in the C_s minimum. These features probably explain why optimization methods found the C_s minimum first;³⁷ the C_{5v} minimum was only discovered relatively recently.³³ Despite this fine structure in the disconnectivity graph, it is still appropriate to say that the icosahedral minima form a single funnel because the minima are structurally very similar and because the barriers are still relatively low and so the minima give rise to a single thermodynamic state.

Another way to visualize the double-funnel topography of the LJ_{38} PES from our set of minima is to plot the energy of the minima against the distance from the global minimum. For a single funnel it is expected that the energy of the minima would generally increase as the distance from the global minimum increases. For a double-funnel PES, going from the global minimum towards the second funnel, the energy first increases as the primary funnel is ascended and then decreases during the descent into the second funnel. Figure 3 clearly shows just such a feature associated with the

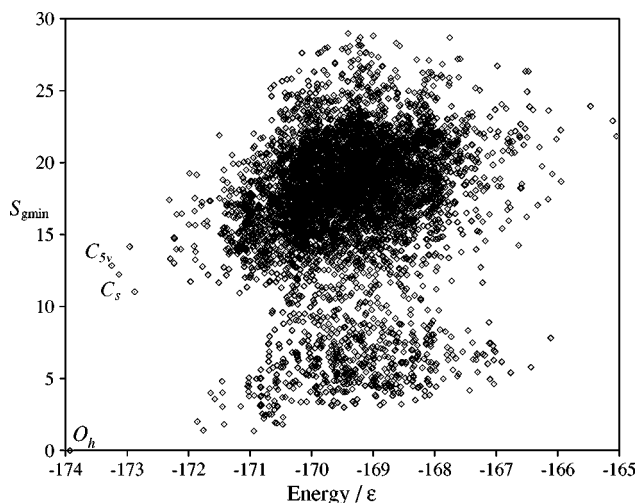


FIG. 3. The dependence of the distance from the global minimum, S_{gmin} , on the potential energy of the minima for a set of 6000 LJ_{38} minima. The points associated with the three lowest-energy minima are labeled by their point groups.

icosahedral funnel, further confirming the double-funnel character of the PES.

The overall picture, therefore, is of a narrow, deep and somewhat rougher funnel containing the global minimum, and a broader, much more voluminous funnel associated with the low-lying icosahedral minimum. The ‘‘rims’’ of both funnels lie in the liquidlike regions of the PES. The greater width of the icosahedral funnel helps to explain why the cluster enters this region of configuration space in the vast majority of annealing simulations. This effect of the funnel width has been previously observed for a model double-funnel PES.⁸

Our sample of minima is clearly only a tiny fraction of the astronomical number available to the system, so we need to consider the possible effects of incompleteness for the disconnectivity graph. As discussed above, from about halfway through the search, very few new structures had lower energy than any of the existing lowest 200. This provides good evidence that the 150 minima actually represented in Fig. 2 really are the lowest. The number of minima represented by higher-energy nodes (for which branches have not been shown) would certainly increase if the search were allowed to proceed for longer.

The incompleteness of the transition state sample is harder to gauge, but has important consequences for the disconnectivity graph. Given an incomplete sample of minima, the graph depends only on transition states that interconnect minima within the sample. Furthermore, two minima may be connected by more than one transition state, but only the lowest matters for the graph because it determines the energy at which the minima become mutually accessible. When a new connectivity is discovered, the pattern of nodes and lines may change significantly. When a lower transition state between two previously connected minima is discovered, branching moves down the graph to lower nodes. In the present work, up to 20 transition state searches were allowed from each minimum, with many of the low-energy minima reaching this limit. A total of 25 403 transition state searches

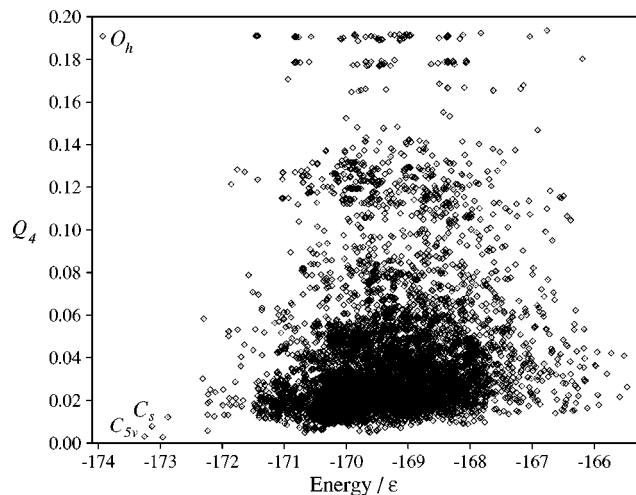


FIG. 4. Q_4 and potential energy values for a set of 6000 LJ₃₈ minima. The points associated with the three lowest-energy minima are labelled by their point groups.

were performed, 21 515 of which converged in a reasonable number of optimization steps. Since only 8 633 transition states were found, most of them must have occurred several times, suggesting that we have an adequate sample, especially as far as the low-energy minima are concerned.

In summary, therefore, we can be quite confident that the disconnectivity graph in Fig. 2 is an accurate representation of the low-energy regions of the PES. This is because it is based on a search that is strongly biased towards low-energy structures, and because the sample of minima and transition states is far larger than the number of branches actually included on the graph.

III. FREE ENERGY LANDSCAPE

As the two funnels are expected to give rise to distinct thermodynamic states, an alternative way of characterizing the double-funnel topography of the LJ₃₈ PES is to compute the free energy as a function of a suitable order parameter. The two funnels would give rise to minima in the free energy which are separated by a barrier. Bond-order parameters, which were initially introduced by Steinhardt *et al.*,⁵³ have been used to characterize the free energy barrier for the nucleation of a crystal from a melt^{54–56} because they can differentiate between the fcc crystal and the liquid. By calculating the bond-order parameters, Q_4 , Q_6 , W_4 and W_6 , for our sample of LJ₃₈ minima we were able to assess whether they might also be used to differentiate the fcc and icosahedral funnels. Both Q_4 and Q_6 appeared suitable and we chose to investigate Q_4 further.

The definition of the order parameter, Q_l , is

$$Q_l = \left(\frac{4\pi}{2l+1} \sum_{m=-l}^l |\bar{Q}_{lm}|^2 \right)^{1/2}, \quad (2)$$

where

$$\bar{Q}_{lm} = \frac{1}{N_b} \sum_{r_{ij} < r_0} Y_{lm}(\theta_{ij}, \phi_{ij}), \quad (3)$$

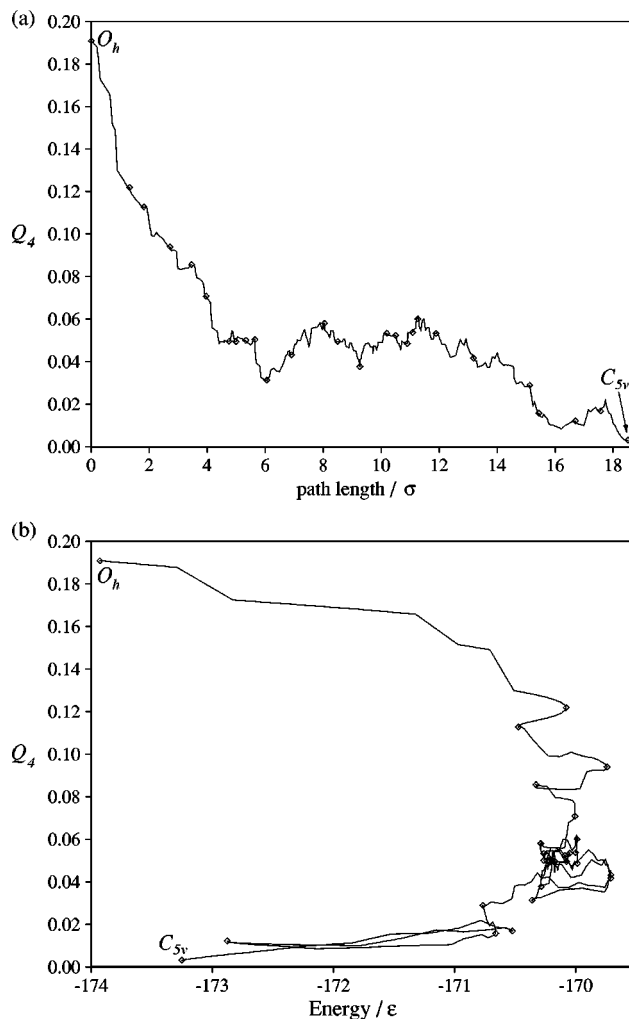


FIG. 5. (a) Q_4 as a function of the distance along the reaction pathway (starting at the global minimum) and (b) Q_4 against potential energy for the lowest energy pathway between the two lowest energy LJ₃₈ minima. The diamonds are for the stationary points (minima and transition states) on the pathway.

where the sum is over all the N_b “bonds” (pairs of atoms which have a pair separation, r_{ij} , which is less than the nearest-neighbor criterion, r_0) in the cluster, $Y_{lm}(\theta, \phi)$ is a spherical harmonic and θ_{ij} and ϕ_{ij} are the polar and azimuthal angles of an interatomic vector with respect to an arbitrary coordinate frame. (Q_l is independent of the choice for this coordinate frame.) We use $r_0 = 1.391\sigma$.

Figure 4 shows that the Q_4 values of the two lowest energy minima are well-separated. However, the large number of minima associated with the liquidlike state have values only slightly greater than those for the icosahedral structures. Therefore, Q_4 is a good order parameter for distinguishing fcc structures but not for differentiating the icosahedral and liquidlike structures.⁵⁷ The similar values of Q_4 for the icosahedral and liquidlike minima reflect structural similarities—both have significant polytetrahedral character.^{26,36}

In Fig. 5 we show the properties of the lowest-energy pathway between the two lowest-energy minima that we found in Sec. II. The value of Q_4 rapidly decreases as the cluster leaves the fcc funnel and enters the liquidlike region

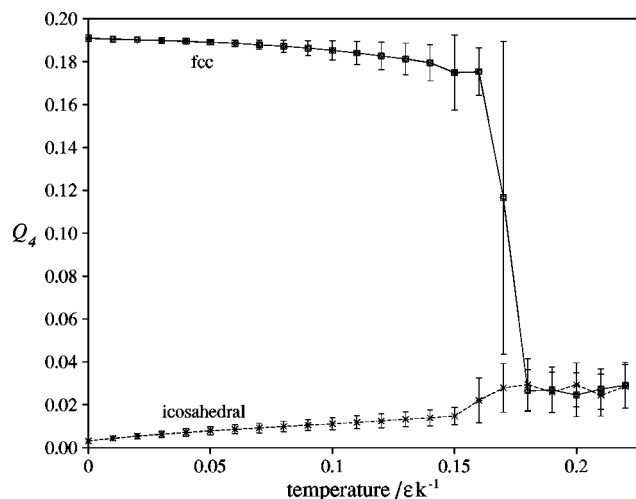


FIG. 6. Q_4 for two series of canonical Monte Carlo runs of increasing temperature. The initial configurations were the fcc global minimum (solid line) and the lowest-energy icosahedral minimum (dashed line). Each point is the average value in a 2×10^6 cycle Monte Carlo run and each run was initiated from the final geometry in the previous lower temperature run. The error bars represent the standard deviation of the Q_4 probability distributions.

of configuration space. A number of rearrangements take place between liquidlike minima before the cluster then enters the icosahedral funnel. From the pathway we can obtain upper bounds to the free energy barriers between the two funnels at zero temperature; the $T=0$ free energy barriers must be less than or equal to 4.22ϵ and 3.54ϵ for fcc to icosahedral and icosahedral to fcc transitions, respectively. These values are upper bounds because there may be lower-energy pathways that we were unable to find. Also the free energy difference between the two minima at $T=0$ is simply the energy difference, 0.68ϵ .

To confirm that Q_4 is not only able to distinguish fcc and icosahedral minima, but also more general configurations from within the two funnels, we performed two series of Monte Carlo simulations of increasing temperature that started from the two lowest energy minima. The probability distributions of Q_4 for the two runs are well separated and do not overlap until the cluster starts to melt at $T \sim 0.17 \epsilon k^{-1}$ (Fig. 6). Below the melting temperature the clusters remain in the funnel in which the simulations were started even when the other funnel has a lower free energy. Hence there is a free energy barrier between the two funnels which is significantly larger than the thermal energy.

In the canonical ensemble the Landau free energy is related to the equilibrium probability distribution of the order parameter by

$$A_L(Q_4) = A - kT \log p_{\text{can}}(Q_4), \quad (4)$$

where A is the Helmholtz free energy. However, conventional simulations are unable to provide equilibrium probability distributions for Q_4 because, as Fig. 6 illustrates, the cluster is unable to pass over the free energy barrier between the two funnels. To overcome this difficulty we use umbrella sampling.⁵⁸ In this method configurations are not sampled with a Boltzmann distribution but with the distribution

$\exp(-\beta E + w(Q_4))$, where $w(Q_4)$ is a biasing potential, the aim of which is to make configurations near the top of the free energy barrier more likely to be sampled. The canonical probability distribution is then obtained from the probability distribution for the biased run, $p_{\text{multi}}(Q_4)$, by

$$p_{\text{can}}(Q_4) = p_{\text{multi}}(Q_4) \exp(-w(Q_4)). \quad (5)$$

We wish to choose w such that $p_{\text{multi}}(Q_4)$ is approximately constant over the whole range of Q_4 (the so-called multicanonical approach^{59,60}). However, this only occurs when $w(Q_4) \approx A_L(Q_4)/kT$ and so we have to construct w iteratively from the results of a number of short preliminary simulations.⁶¹

We were able to compute $A_L(Q_4)$ successfully for $T \geq 0.15 \epsilon k^{-1}$. However, at lower temperatures, even with a reasonable biasing distribution, the rate at which the system passed between the two funnels was too low for accurate free energies to be obtained. At the top of the free energy barrier in this temperature range the contribution of states which mediate transitions between the two funnels is small (instead the contribution of other lower-energy states dominates), and so even at the top of the barrier a transition to the other funnel is an activated process. To overcome this difficulty would require either unfeasibly long simulations or a better order parameter for which the contribution of irrelevant states to the free energy barrier region is less. However, the results we obtain are sufficient to give us a good picture of the free energy landscape of LJ_{38} .

In our simulations we collected the values of Q_4 and E_c (the configurational, or potential, energy) into a two-dimensional histogram. This approach allows us to obtain the two-dimensional free energy surface, $A_L(Q_4, E_c)$ (Fig. 7), as well as the free energy profile, $A_L(Q_4)$ [Fig. 8(a)]. Furthermore, it allows us to decompose $A_L(Q_4)$ into its energetic and entropic components,

$$A_L(Q_4) = E_{c,L}(Q_4) - TS_L(Q_4), \quad (6)$$

because we can obtain $E_{c,L}(Q_4)$ from our two-dimensional probability distribution using

$$E_{c,L}(Q_4) = \int p_{\text{can}}(Q_4, E_c) E_c dE_c. \quad (7)$$

Moreover, we can apply the histogram method⁶² to calculate results for temperatures other than those at which we performed simulations. As

$$p(Q_4, E_c; \beta) = \Omega_c(Q_4, E_c) \exp(-\beta E_c) / Z(\beta), \quad (8)$$

where $\Omega_c(Q_4, E_c)$ is related to the configurational density of states by $\Omega_c(E_c) = \int \Omega_c(Q_4, E_c) dQ_4$ and $Z(\beta)$ is the partition function, it follows that

$$p(Q_4, E_c; \beta') \propto p(Q_4, E_c; \beta) \exp(-E_c(\beta' - \beta)), \quad (9)$$

where β is the reciprocal temperature of the original simulation and β' is the reciprocal temperature to which the results have been extrapolated. This method, though, has to be applied with a certain amount of caution since the extrapolation becomes increasingly sensitive to statistical errors at the edge of the $p(Q_4, E_c; \beta)$ distribution (Fig. 7) as the difference in temperature increases.⁶³

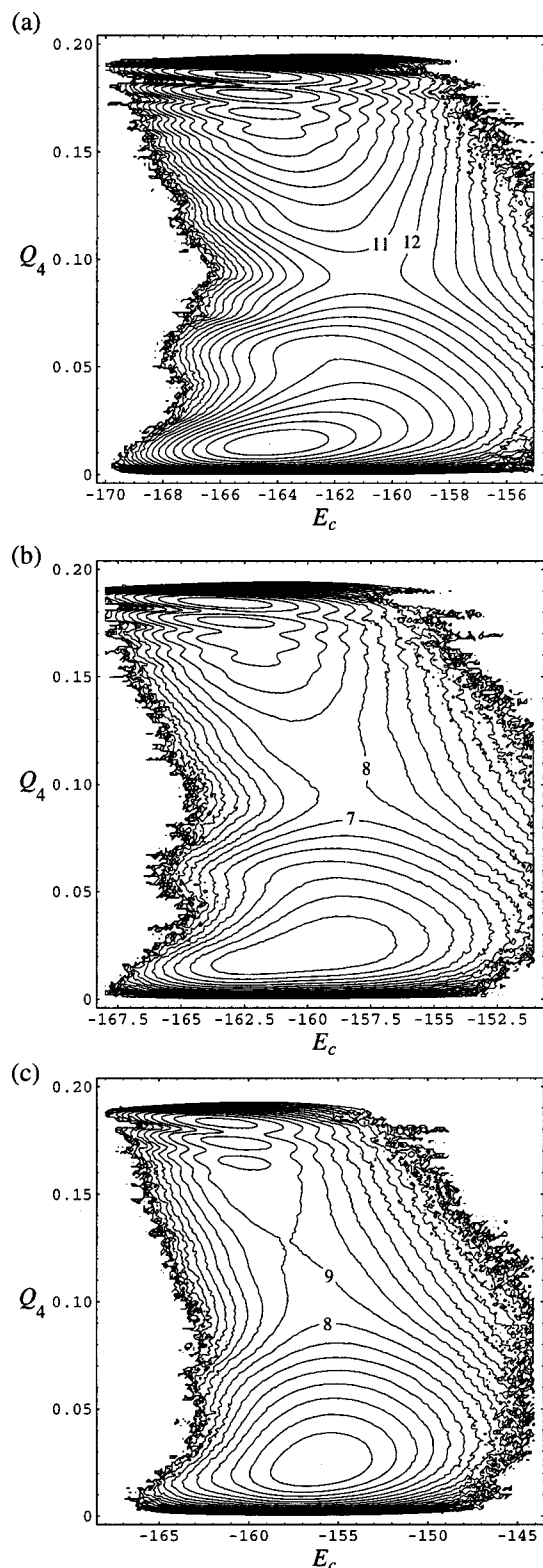


FIG. 7. Contour plots of $A_L(Q_4, E_c)$ at temperatures of (a) $0.15 \epsilon k^{-1}$, (b) $0.18 \epsilon k^{-1}$, and (c) $0.21 \epsilon k^{-1}$. The contours are spaced $1 kT$ apart. The free energy zero is the bottom of the icosahedral/liquidlike free energy minimum. Near to the free energy transition state some of the contours have been labeled by the value of the free energy in kT . No points were sampled in the regions free of contours. The results are from Monte Carlo runs of (a) 250×10^6 , (b) 20×10^6 , and (c) 15×10^6 cycles.

At $T = 0.15 \epsilon k^{-1}$ the free energy profile has two main minima (the one at $Q_4 = 0.015$ corresponding to the icosahedral funnel and the one at $Q_4 = 0.186$ corresponding to the fcc funnel) which are separated by a barrier [Fig. 8(a)].

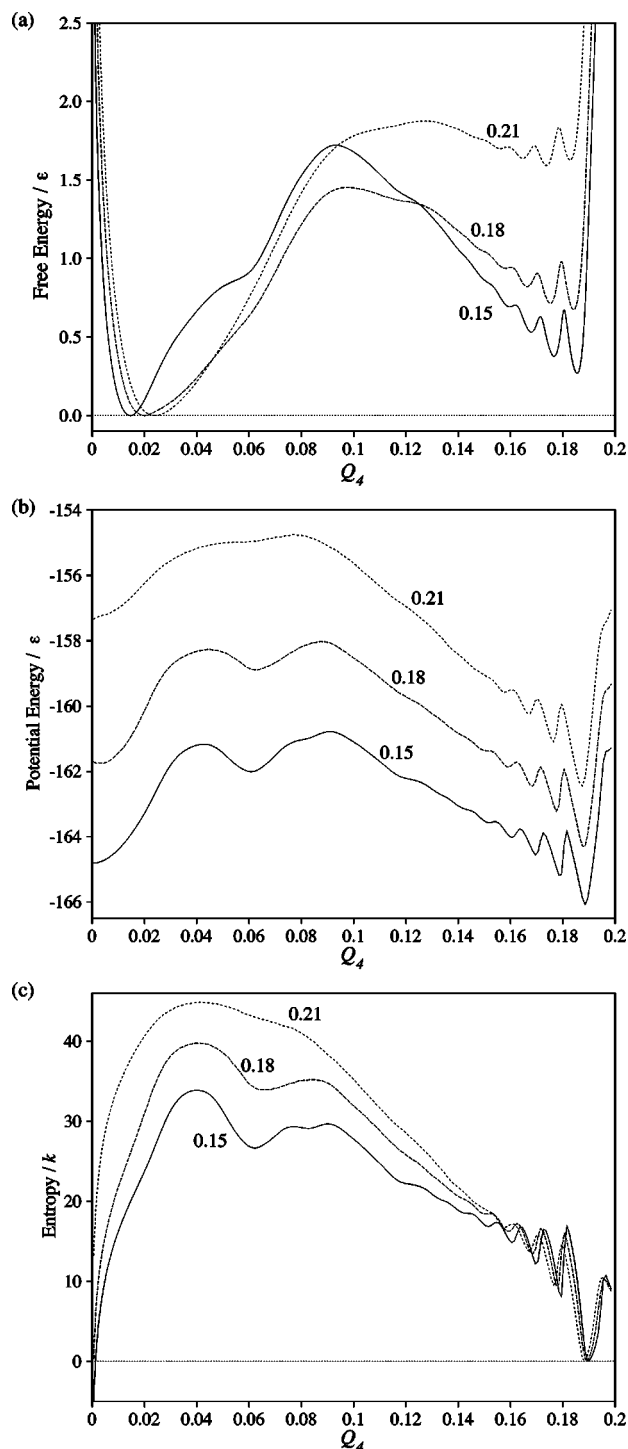


FIG. 8. (a) $A_L(Q_4)$, (b) $E_{c,L}(Q_4)$, and (c) $S_L(Q_4)$ at three different temperatures, as labeled (in units of ϵk^{-1}). We have chosen the low Q_4 free energy minimum as the zero of A_L and the lowest value of S_L in the fcc funnel as the zero of S_L .

Around the fcc free energy minimum there are a number of oscillations in $A_L(Q_4)$. These are a result of the discontinuities that occur in the order parameter when the value of an interatomic distance passes through r_0 and do not indicate that there are small free energy barriers between different fcc structures. These discontinuities can also be seen in the pathway in Fig. 5 at large values of Q_4 .

At $T=0.15 \text{ } \epsilon k^{-1}$ the icosahedral funnel is lower in free energy because it has a larger entropy [Figs. 8(c) and 9(a)] due to the larger number of icosahedral minima (Fig. 2) and their lower mean vibrational frequency.^{34,35} The free energy barrier is large with respect to the thermal energy (11.5 and $9.69 kT$ with respect to the free energy minima) and relative to kT increases rapidly as the temperature decreases [Fig. 10(b)]. The size of the barrier explains why, below the melting temperature, simulations are trapped in one well or the other.

Examining Fig. 9(a) shows that at $T=0.15 \text{ } \epsilon k^{-1}$ the free energy barrier is energetic in origin, and that the larger entropy of the intermediate states acts to reduce the magnitude of the barrier. As the temperature decreases, this entropic contribution decreases and so the barrier (in absolute terms) increases until it reaches its purely energetic value at zero temperature. The histogram approach allows an estimate of the position of the fcc to icosahedral transition. It predicts that the free energy difference between the two funnels is zero at $T=0.118 \text{ } \epsilon k^{-1}$ (Fig. 10) which is in good agreement with the thermodynamic results obtained using the superposition method.³⁵

As the temperature increases from $T=0.15 \text{ } \epsilon k^{-1}$ the liquidlike state makes an increasing contribution to the low Q_4 free energy minimum. For example, the value of Q_4 at the minimum gradually increases [Figs. 8(a) and 10(c)], reflecting the slightly larger values of Q_4 for the liquidlike state (Fig. 4) and the minimum becomes broader. At $T=0.18 \text{ } \epsilon k^{-1}$ in a canonical simulation the cluster passes back and forth between the liquidlike and icosahedral states in time. This dynamical coexistence is reflected in the low Q_4 free energy minimum of $A_L(Q_4, E_c)$ —comparison of Fig. 7(b) to Figs. 7(a) and 7(c) shows that it is a superposition of two states.

At $T=0.21 \text{ } \epsilon k^{-1}$ the low Q_4 free energy minimum is solely due to the liquidlike state and the free energy landscape is dominated by the free energy difference between the fcc and liquidlike structures which results from the much larger entropy of the liquid [Fig. 8(c)]. The fcc free energy minimum is now shallow and the flatness of the free energy landscape for $Q_4 > 1.0$ is a result of the compensation of the energy and entropic components [Fig. 9(c)]. The histogram approach predicts that the fcc free energy minimum finally disappears at $T \sim 0.235 \text{ } \epsilon k^{-1}$ (Fig. 10).

The free energy barrier to pass from the low Q_4 free energy minimum to the fcc funnel has an interesting temperature dependence (Fig. 10). It has a minimum at a temperature close to the melting transition. Below this temperature the barrier increases because of the decreasing effect of the entropy of intermediate states in reducing the energetic barrier between the two free energy minima. Above this temperature the barrier increases because of the increasing free energy difference between the two minima. As a canonical simulation is most likely to enter the fcc funnel when the free energy barrier relative to the thermal energy is at its smallest, the optimum temperature for reaching the basin of attraction of the fcc global minimum is $T \sim 0.19 \text{ } \epsilon k^{-1}$ [Fig. 10(b)]. This result is somewhat counterintuitive because one would usually expect the optimum temperature to occur when the equi-

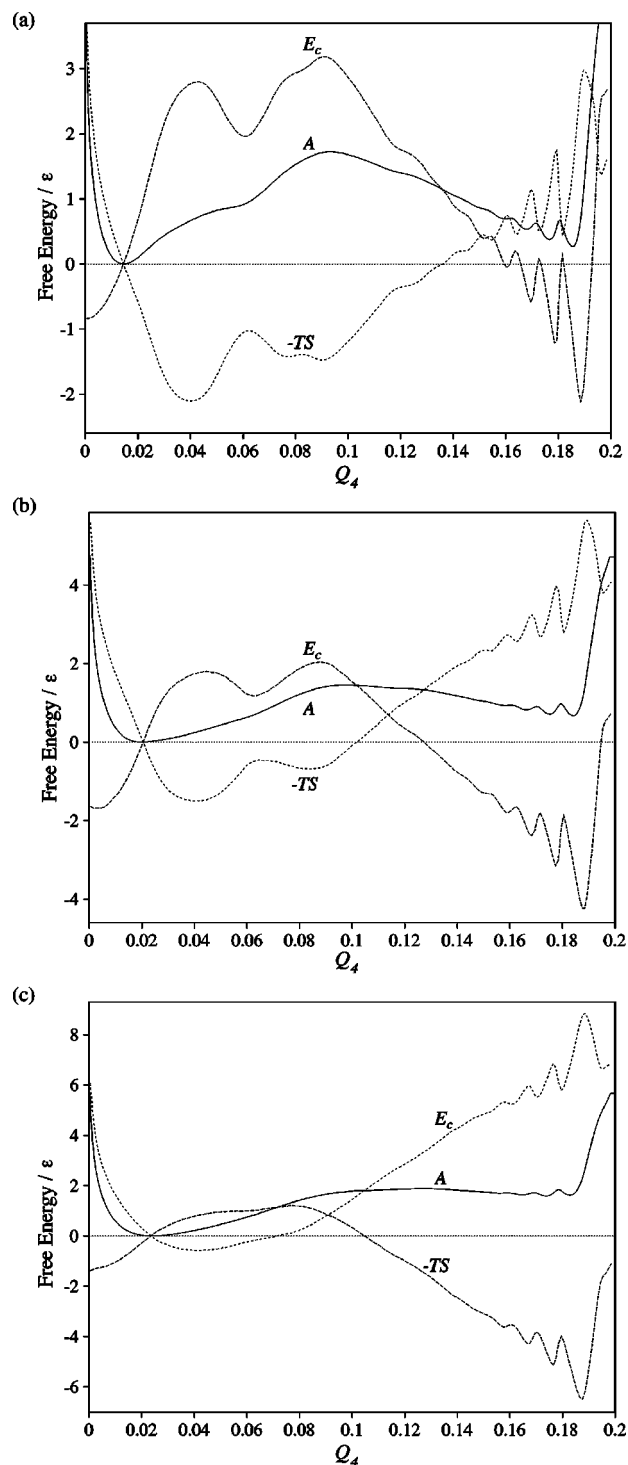


FIG. 9. The decomposition of the free energy profiles $A_L(Q_4)$ (solid line) into their energetic ($E_{c,L}(Q_4)$ [dashed line]) and entropic ($-TS_L(Q_4)$ [dotted line]) contributions at temperatures of (a) $0.15 \text{ } \epsilon k^{-1}$, (b) $0.18 \text{ } \epsilon k^{-1}$, and (c) $0.21 \text{ } \epsilon k^{-1}$. The zeros of all three quantities have been set to occur at the position of the low Q_4 free energy minimum.

librium probability of being in the basin of attraction of the global minimum is higher; $p_{O_h}^{\text{eq}} = 0.004$ at $T=0.19 \text{ } \epsilon k^{-1}$.³⁵ Figure 11 does indeed confirm that a simulation at this temperature can enter the fcc funnel, albeit rarely. The cluster enters the fcc funnel once in 1.5×10^7 Monte Carlo cycles and remains there for $\sim 150\,000$ cycles.

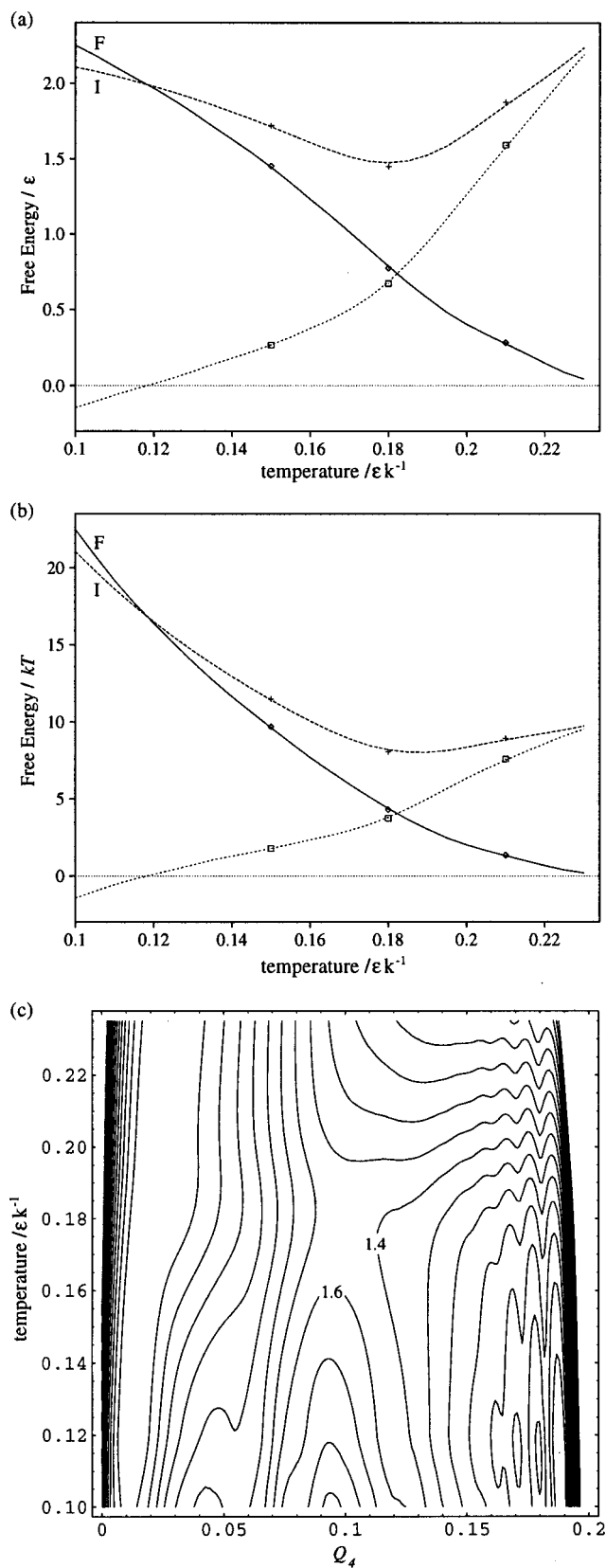


FIG. 10. (a) and (b) The height of the free energy barrier relative to the fcc (F) and low Q_4 (I) free energy minima and the free energy difference (dotted line) between the two free energy minima as a function of temperature. The points are derived from the simulation profiles and the lines result from using a histogram method. (c) Two-dimensional contour plot showing the temperature dependence of the free energy landscape, $A_L(Q_4, T)$. At each temperature we have set the zero of the free energy to that of the lower free energy minimum. The units of free energy are ϵ in (a) and (c), and kT in (b). The contours in (c) are at a spacing of 0.2ϵ .

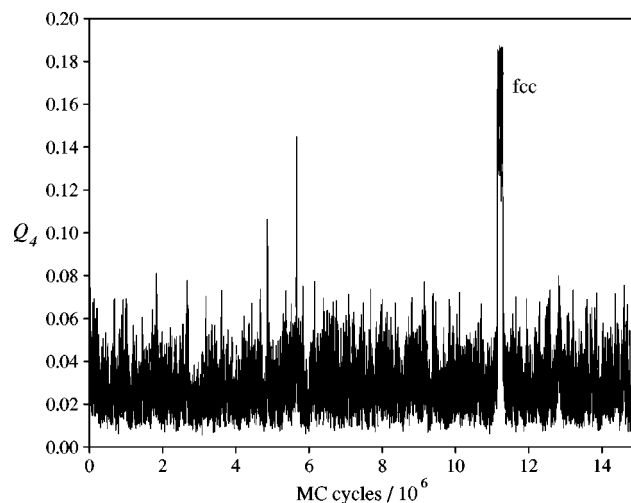


FIG. 11. Q_4 during a canonical Monte Carlo run at $T=0.19 \epsilon k^{-1}$. The label shows the short section of the simulation where the fcc funnel is entered.

The order parameter Q_4 does not allow us to obtain the free energy barrier between the icosahedral and liquidlike states. However, it must be considerably smaller than the barrier for passage from the liquidlike state to the fcc funnel, as dynamical coexistence of the two states is seen over a wide range of temperature. For LJ₅₅ E_c is able to detect a free energy barrier between the Mackay icosahedron and the liquid,⁵⁷ but for LJ₃₈ $p(E_c)$ is unimodal. However, $p(Q_6)$ has distinct maxima corresponding to icosahedral and liquidlike states in the region of the melting transition (Fig. 12); the separate maxima disappear above $T=0.19 \epsilon k^{-1}$. At $T=0.18 \epsilon k^{-1}$ these maxima give rise to a free energy barrier of $0.93 kT$ for passing from the liquidlike state into the icosahedral funnel. This compares to a value of $8.08 kT$ for passing into the fcc funnel. This difference is consistent with the picture of the energy landscape obtained from the disconnectivity graph that showed the fcc funnel to be much narrower (and therefore less accessible); it probably results from the greater structural similarity between the icosahedral and liq-

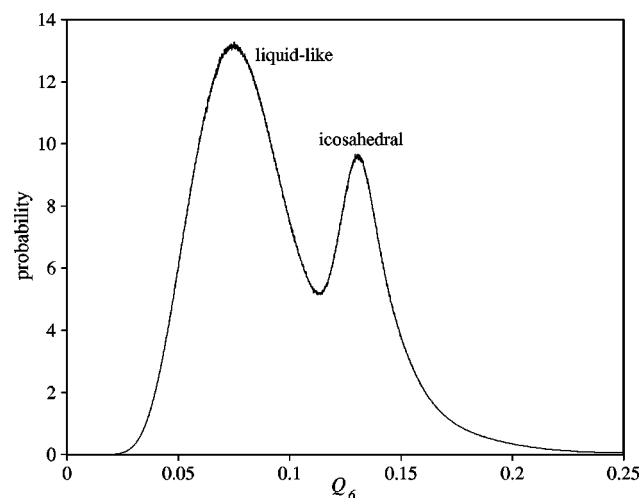


FIG. 12. Probability distribution of Q_6 during a Monte Carlo run at $T=0.18 \epsilon k^{-1}$.

liquidlike states. This result clearly explains why the LJ₃₈ cluster is much more likely to enter the icosahedral funnel on relaxation down the PES.

IV. CONCLUSIONS

The disconnectivity graph and free energy profiles that we have computed in this paper provide an integrated picture of the energy landscape of LJ₃₈. Both methods clearly confirm that the PES has two funnels. The fcc funnel is deep and narrow and terminates at the truncated octahedral global minimum. The icosahedral funnel is much wider and has a flatter bottom. The large energy barrier between the two funnels gives rise to a large free energy barrier that causes the cluster to be trapped in one of the funnels when the temperature is below the melting point. Furthermore, the difference in the width of the funnels leads to a much lower free energy barrier for passage from the liquidlike state into the icosahedral funnel. This explains why the cluster preferentially enters the icosahedral funnel on cooling and why global optimization of this cluster is difficult using those methods that do not transform the energy landscape.

LJ₃₈ has a paradigmatic double-funnel energy landscape and so our understanding of this cluster can help provide insight into other systems for which a number of funnels may be present on the PES. There is a clear relationship between multiple funnels and trapping, and we saw for LJ₃₈ that the free energy barriers between low-energy structures in different funnels increase relative to the thermal energy as the temperature decreases. In glass-forming systems we expect that the glass transition is the result of similar increases in free energy barriers between different low-energy amorphous structures. It would therefore be very interesting to use disconnectivity graphs to probe the multiple-funnel structure of the energy landscapes of model glasses. As water is a ‘‘strong’’ liquid the disconnectivity graph that has been obtained for (H₂O)₂₀ may provide a clue to what one might expect.⁴²

The trapping that results from multiple funnels on the energy landscape also clearly shows why it is important that proteins have a single accessible funnel.⁷ Trapping in a non-native funnel would prevent the protein from performing its biological function. Our results for LJ₃₈ also suggest the possibility that the native state might not always correspond to the free energy global minimum. There could be some cases where the funnel leading down to the global minimum is so narrow that it is inaccessible on most time scales.⁸ The folding of the protein would then be associated with trapping in a more accessible funnel, and the functional lifetime of the protein would depend on the rate of escape from this funnel to the global minimum. Indeed, there are some proteins from the serpin family of protease inhibitors for which this seems to occur.⁶⁴ For example, the protein plasminogen activator inhibitor-1 first folds to the active state, but then on a time scale of hours can spontaneously transform to an inactive latent form.^{65,66} However, this scenario is likely to be the exception rather than the rule.

We found that the ease of reaching the global minimum on a multiple-funnel energy landscape is related to the free

energy barriers for entering the different funnels from the liquid, which in turn are related to the width of the funnels. Our results, therefore, add weight to the intuitive picture that glass-formers have a narrow funnel leading down to the crystal. These features of the energy landscape are intimately related to the structure. For example, in LJ₃₈ the greater accessibility of the liquidlike state can also be explained in terms of the greater structural similarity of the liquid to the icosahedral structures (both have some polytetrahedral character) than to the fcc structures. Similarly, Straley found that crystallization to a bulk close-packed structure in flat space is much more difficult than to the completely polytetrahedral {3,3,5} polytope in a positively-curved space (the three-dimensional hypersurface of a four-dimensional sphere) where this structure is the global minimum.⁶⁷

ACKNOWLEDGMENTS

D.J.W. is grateful to the Royal Society and M.A.M. to the Engineering and Physical Sciences Research Council for financial support. The work of the FOM Institute is part of the scientific program of FOM and is supported by the Nederlandse Organisatie voor Wetenschappelijk Onderzoek (NWO).

- ¹A. Sali, E. Shakhnovich, and M. Karplus, *Nature (London)* **369**, 248 (1994).
- ²A. Sali, E. Shakhnovich, and M. Karplus, *J. Mol. Biol.* **235**, 1614 (1994).
- ³D. K. Klimov and D. Thirumalai, *Phys. Rev. Lett.* **76**, 4070 (1996).
- ⁴H. Li, R. Helling, C. Tang, and N. S. Wingreen, *Science* **273**, 666 (1996).
- ⁵R. Mélin, H. Li, N. S. Wingreen, and C. Tang, *J. Chem. Phys.* **110**, 1252 (1999).
- ⁶P. E. Leopold, M. Montal, and J. N. Onuchic, *Proc. Natl. Acad. Sci. USA* **89**, 8271 (1992).
- ⁷J. D. Bryngelson, J. N. Onuchic, N. D. Socci, and P. G. Wolynes, *Proteins: Struct., Funct., Genet.* **21**, 167 (1995).
- ⁸J. P. K. Doye and D. J. Wales, *J. Chem. Phys.* **105**, 8428 (1996).
- ⁹R. Zwanzig, A. Szabo, and B. Bagchi, *Proc. Natl. Acad. Sci. USA* **89**, 20 (1992).
- ¹⁰R. Zwanzig, *Proc. Natl. Acad. Sci. USA* **92**, 9801 (1995).
- ¹¹M. Cieplak, M. Henkel, J. Karbowski, and J. R. Banavar, *Phys. Rev. Lett.* **80**, 3654 (1998).
- ¹²R. Czerminski and R. Elber, *J. Chem. Phys.* **92**, 5580 (1990).
- ¹³O. M. Becker and M. Karplus, *J. Chem. Phys.* **106**, 1495 (1997).
- ¹⁴Y. Levy and O. M. Becker, *Phys. Rev. Lett.* **81**, 1126 (1998).
- ¹⁵R. S. Berry, N. Elmaci, J. P. Rose, and B. Vekhter, *Proc. Natl. Acad. Sci. USA* **94**, 9520 (1997).
- ¹⁶J. N. Onuchic, P. G. Wolynes, Z. Luthey-Schulten, and N. D. Socci, *Proc. Natl. Acad. Sci. USA* **92**, 3626 (1995).
- ¹⁷N. D. Socci, J. N. Onuchic, and P. G. Wolynes, *J. Chem. Phys.* **104**, 5860 (1996).
- ¹⁸F. H. Stillinger and T. A. Weber, *Science* **225**, 983 (1984).
- ¹⁹C. A. Angell, *Science* **267**, 1924 (1995).
- ²⁰F. H. Stillinger, *Science* **267**, 1935 (1995).
- ²¹S. Sastry, P. G. Debenedetti, and F. H. Stillinger, *Nature (London)* **393**, 554 (1998).
- ²²L. Angelani, G. Parisi, G. Ruocco, and G. Vilianni, *Phys. Rev. Lett.* **81**, 4648 (1998).
- ²³G. T. Barkema and N. Mousseau, *Phys. Rev. Lett.* **81**, 1865 (1998).
- ²⁴M. R. Hoare and J. McInnes, *Faraday Discuss. Chem. Soc.* **61**, 12 (1976).
- ²⁵C. J. Tsai and K. D. Jordan, *J. Phys. Chem.* **97**, 11227 (1993).
- ²⁶J. P. K. Doye and D. J. Wales, *J. Phys. B* **29**, 4859 (1996).
- ²⁷M. A. Miller, J. P. K. Doye, and D. J. Wales, *J. Chem. Phys.* **110**, 328 (1999).
- ²⁸D. J. Wales and R. S. Berry, *J. Chem. Phys.* **92**, 4283 (1990).
- ²⁹M. A. Miller and D. J. Wales, *J. Chem. Phys.* **107**, 8568 (1997).
- ³⁰A. L. Mackay, *Acta Crystallogr.* **15**, 916 (1962).

- ³¹J. P. K. Doye, D. J. Wales, and R. S. Berry, *J. Chem. Phys.* **103**, 4234 (1995).
- ³²J. Pillardy and L. Piela, *J. Phys. Chem.* **99**, 11805 (1995).
- ³³D. M. Deaven, N. Tit, J. R. Morris, and K. M. Ho, *Chem. Phys. Lett.* **256**, 195 (1996).
- ³⁴J. P. K. Doye and D. J. Wales, *Phys. Rev. Lett.* **80**, 1357 (1998).
- ³⁵J. P. K. Doye, D. J. Wales, and M. A. Miller, *J. Chem. Phys.* **109**, 8143 (1998).
- ³⁶D. R. Nelson and F. Spaepen, *Solid State Phys.* **42**, 1 (1989).
- ³⁷J. A. Northby, *J. Chem. Phys.* **87**, 6166 (1987).
- ³⁸D. J. Wales and J. P. K. Doye, *J. Phys. Chem. A* **101**, 5111 (1997).
- ³⁹R. H. Leary, *J. Global Optim.* **11**, 35 (1997).
- ⁴⁰J. A. Niesse and H. R. Mayne, *J. Chem. Phys.* **105**, 4700 (1996).
- ⁴¹C. Barrón, S. Gómez, and D. Romero, *Appl. Math. Lett.* **9**, 75 (1996).
- ⁴²D. J. Wales, M. A. Miller, and T. R. Walsh, *Nature (London)* **394**, 758 (1998).
- ⁴³J. Pancfř, *Collect. Czech. Chem. Commun.* **40**, 1112 (1974).
- ⁴⁴C. J. Cerjan and W. H. Miller, *J. Chem. Phys.* **75**, 2800 (1981).
- ⁴⁵D. J. Wales, *J. Chem. Phys.* **101**, 3750 (1994).
- ⁴⁶M. Page and J. W. McIver, *J. Chem. Phys.* **88**, 922 (1988).
- ⁴⁷J. P. K. Doye and D. J. Wales, *Z. Phys. D* **40**, 194 (1997).
- ⁴⁸G. T. Barkema and N. Mousseau, *Phys. Rev. Lett.* **77**, 4358 (1996).
- ⁴⁹N. Mousseau and G. T. Barkema, *Phys. Rev. E* **57**, 2419 (1998).
- ⁵⁰T. R. Walsh and D. J. Wales, *J. Chem. Phys.* **109**, 6691 (1998).
- ⁵¹J. P. K. Doye and D. J. Wales, *Phys. Rev. B* **59**, 2292 (1999).
- ⁵²M. A. Miller, J. P. K. Doye, and D. J. Wales (in preparation).
- ⁵³P. J. Steinhardt, D. R. Nelson, and M. Ronchetti, *Phys. Rev. B* **28**, 784 (1983).
- ⁵⁴J. S. van Duijneveldt and D. Frenkel, *J. Chem. Phys.* **96**, 4655 (1992).
- ⁵⁵P. R. ten Wolde, M. J. Ruiz-Montero, and D. Frenkel, *Phys. Rev. Lett.* **75**, 2714 (1995).
- ⁵⁶P. R. ten Wolde, M. J. Ruiz-Montero, and D. Frenkel, *J. Chem. Phys.* **104**, 9932 (1996).
- ⁵⁷R. M. Lynden-Bell and D. J. Wales, *J. Chem. Phys.* **101**, 1460 (1994).
- ⁵⁸G. M. Torrie and J. P. Valleau, *Chem. Phys. Lett.* **28**, 578 (1974).
- ⁵⁹B. A. Berg and T. Neuhaus, *Phys. Lett. B* **267**, 249 (1991).
- ⁶⁰B. A. Berg and T. Neuhaus, *Phys. Rev. Lett.* **69**, 9 (1992).
- ⁶¹B. A. Berg, *J. Stat. Phys.* **82**, 323 (1996).
- ⁶²I. R. McDonald and K. Singer, *Discuss. Faraday Soc.* **43**, 40 (1967).
- ⁶³M. E. J. Newman and R. G. Palmer (cond-mat/9804306).
- ⁶⁴D. Baker and D. A. Agard, *Biochemistry* **33**, 7505 (1994).
- ⁶⁵A. E. Franke, D. E. Danley, F. S. Kaczmarek, S. J. Hawrylik, R. D. Gerard, S. F. Lee, and K. F. Geoghegan, *Biochim. Biophys. Acta* **1037**, 16 (1990).
- ⁶⁶R. W. Carrell, D. L. Evans, and P. E. Stein, *Nature (London)* **353**, 576 (1991).
- ⁶⁷J. P. Straley, *Phys. Rev. B* **30**, 6592 (1984).